corrosion and materials degradation

MDPI

Article

Cathodic Protection of Carbon Steel in Soil: A Study of Induced Passivation

Philippe Refait [1,*], Marc Jeannin [1], Elisabeth Fleury [2], Florian Raffin [2] and Sylvain Fontaine [3]

[1] Laboratory of Engineering Sciences for the Environment (LaSIE)—UMR CNRS 7356, La Rochelle University, 17000 La Rochelle, France; mjeannin@univ-lr.fr
[2] RICE—Research & Innovation Center for Energy, 92390 Villeneuve-la-Garenne, France; elisabeth.fleury@grtgaz.com (E.F.); florian.raffin@external.grtgaz.com (F.R.)
[3] GRTgaz, 60200 Compiègne, France; sylvain.fontaine@grtgaz.com
* Correspondence: prefait@univ-lr.fr; Tel.: +33-5-46-45-82-27

Abstract: Two-month experiments were carried out with carbon steel electrodes buried in an artificial sand wetted at 50–55% of saturation with a 0.07 mol L^{-1} $Na_2SO_4 \cdot 10H_2O$ solution. Various protection potentials (corrected from the ohmic drop) were applied from −0.60 to −1.13 V/Cu-$CuSO_4$. In each case, the behavior of the electrode protected by cathodic polarization was compared with that of an unprotected electrode. The electrochemical study was performed using voltammetry, linear polarization resistance measurements, and EIS. Surface characterization of the coupons was carried out using optical microscopy and X-ray diffraction. First, cathodic protection was observed to induce a spreading of the electrolyte on the metal surface because of electrocapillary effects. The active area, or more precisely the wet area, of the electrode increased, leading to a decrease in soil electrolyte resistance R_s measured using EIS. This phenomenon was experimentally confirmed via visual observations of the surface of the coupons at the end of the experiments. Secondly, cathodic protection induced a passivation of the steel surface. The passive state persisted for 35 to 85 h after cathodic protection was stopped and could be studied during various periods of interruption of the protection. In each case, the OCP of the previously polarized coupons reached high values, actually 200–250 mV higher than those measured for the unprotected coupons, and was associated with high polarization resistance R_p values (~40 kΩ cm^2). Depassivation of the metal finally occurred, a phenomenon revealed by simultaneous important drops of both OCP and R_p.

Keywords: buried steel pipelines; cathodic protection; passivation; soil; EIS

Citation: Refait, P.; Jeannin, M.; Fleury, E.; Raffin, F.; Fontaine, S. Cathodic Protection of Carbon Steel in Soil: A Study of Induced Passivation. *Corros. Mater. Degrad.* **2024**, *5*, 387–405. https://doi.org/10.3390/cmd5030017

Academic Editor: Jamie Quinton

Received: 3 July 2024
Revised: 31 July 2024
Accepted: 28 August 2024
Published: 31 August 2024

1. Introduction

Buried steel pipes used to transport natural gas are commonly protected against corrosion by the combination of an organic coating with cathodic protection (CP). The coating acts primarily as a physical barrier isolating the metal from the corrosive environment, while CP ensures the protection of the bare areas of the metal surface that result from pores, cracks, and other coating defects. According to relevant international standard EN ISO 15589-1:2017 [1], CP should lead to a residual corrosion rate smaller than 10 µm yr^{-1} provided that the applied cathodic potential is below a threshold value of −850 mV/Cu-$CuSO_4$ (for most soil conditions). Various studies were devoted to the estimation of the residual corrosion rate, being the low corrosion rate achieved with CP, using voltammetry [2–6], and confirmed that the residual corrosion rate was indeed smaller or equal to the expected value of 10 µm yr^{-1}.

The effectiveness of CP can be explained by two main mechanisms [7]. The first mechanism is linked to the electrode kinetic theory, which shows that the decrease in the potential directly induces a decrease in the anodic reaction rate, and thus a decrease in the corrosion rate. However, the decrease in the potential also induces an increase in the cathodic reaction rate and thus an increase in the interfacial pH. The pH was,

for instance, measured up to 11.8 at a steel/clay soil interface after CP was applied at −850 mV/Cu-$CuSO_4$ [8] and up to 13.5 at a steel/sandy soil interface with a CP potential of −950 mV/Cu-$CuSO_4$ [9]. This increase in interfacial pH may lead to the passivation of the steel surface. With this second mechanism, the decrease in the corrosion rate would be mainly due to the formation of a thin protective iron oxide layer, i.e., a passive film. Passivation could be, in most cases, the main mechanism involved for the CP of carbon steel buried in soils [10–12]. It must also be noted that various proposed mechanisms for AC corrosion are based on the presence of a CP-induced passive layer [13,14]. AC corrosion is a phenomenon associated with alternating current (AC) interferences that affect CP-protected buried steel structures. The first step of AC corrosion could correspond to the weakening and breakdown of the CP-induced passive film because of electromechanical stress induced by the AC interference [15,16].

Understanding this CP-induced passivation phenomenon and determining the protective ability of the obtained passive layer is therefore of utmost importance, but the literature data about this topic is scarce. Leeds and Cottis showed, for instance, that, in conditions preventing the formation of the calcareous deposit (NaCl solution), CP induced the formation of a protective layer [17]. The most protective layer was mainly composed of magnetite and was obtained for an applied potential of −1.3 V/Ag-AgCl-3.5% NaCl that led to a pH of 12.74 after 30 days [17]. It is important to keep in mind that CP decreases the corrosion rate, but does not completely halt corrosion, whatever the applied potential [18]. This residual corrosion process can actually lead to (and was evidenced by) the formation of a thin film of corrosion products [17–20].

However, as far as buried structures are concerned, it is necessary to take into account the main differences between the bulk electrolyte and soil, which is a porous medium that restricts the transport of matter. In saturated soils, the transport of dissolved O_2 can only be achieved by diffusion [21,22] inside a pore network that may be extremely tortuous, and corrosion rates are generally very low in such a situation [22–24]. In unsaturated soils, typically below 75% of the saturation level, O_2 can also be transported inside the pores in the gas phase, and important corrosion rates can be reached, with a maximum associated with a specific saturation level that depends on the considered kind of soil [25]. In addition, part of a steel surface buried in unsaturated soil is in contact with the gas phase so that only the fraction of the surface in contact with the electrolyte, which can be called the wet area, is actually corroding. If the wet area is not determined, corrosion rates deduced using the whole metal surface are then underestimated [23,24]. The wet area can be evaluated using electrochemical impedance spectroscopy (EIS) [4,23,24]. Basically, the soil electrolyte resistance R_s, a parameter easily obtained via EIS measurements, varies conversely to the wet area [4,23,24].

Moreover, unsaturated soils may be heterogeneous, with variable local moisture, so that the relevant parameter is not the average saturation level, but the local saturation level at the steel/soil interface [26]. The soil electrolyte resistance R_s is then also an indicator of the local soil moisture at the steel/electrolyte interface, a concept that was recently applied to monitor the evolution of a steel/soil interface during soil drying and re-wetting using a multi-coupon electrode [26].

Finally, the influence of CP on the steel/soil interface must also be taken into account. Previous studies [4,5] indicated that CP increased the wet area through electrocapillary effects that modify the liquid/solid contact angle at the triple phase (gas/liquid/solid) boundary [27–30]. Therefore, the present study, focused on CP induced passivation, was carried out using complementary electrochemical methods, namely voltammetry to follow the evolution of steel during CP, linear polarization measurements (LPR) to assess for the passive state of the steel surface after stopping the cathodic polarization, and EIS measurements to follow, via the R_s parameter, the evolution of the wet area of carbon steel electrodes. The exact relationship between R_s and the wet area is not clearly established yet, and thus R_s was only used in the present study as a qualitative and reliable parameter

linked to the wet area, i.e., a small R_s means a large wet area and a large R_s means a small wet area.

The behavior of electrodes protected using CP was compared with the behavior of unprotected electrodes. At the end of the experiments, a surface analysis was performed using X-ray diffraction (XRD) to identify the phases formed on the steel surface and optical microscopy (OM) to quantify the localized corrosion damage.

2. Materials and Methods

2.1. Materials

Cylindrical Plexiglas cells (25 cm high, 19 cm diameter) filled with 9 kg of wetted soil were used (Figure 1). Each cell comprised a moisture sensor, a $Cu/CuSO_4$ saturated reference electrode (Celco 5, from COREXCO, Décines Charpieu, France, E = +0.317 V/SHE at 25 °C [31]), a titanium counter electrode, and two X70 carbon steel working electrodes, one left unprotected at the open circuit potential (OCP), the other subjected to CP. The composition of the X70 steel used for this study, provided and analyzed by GRTgaz (Compiègne, France), was (in wt.%): 0.09% C, 1.53% Mn, 0.29% Si, 0.013% P, 0.002% S, 0.02% V, 0.03% Cr, 0.03% Cu, 0.03% Ni, 0.03% Al, <0.01% Mo and Fe (balance).

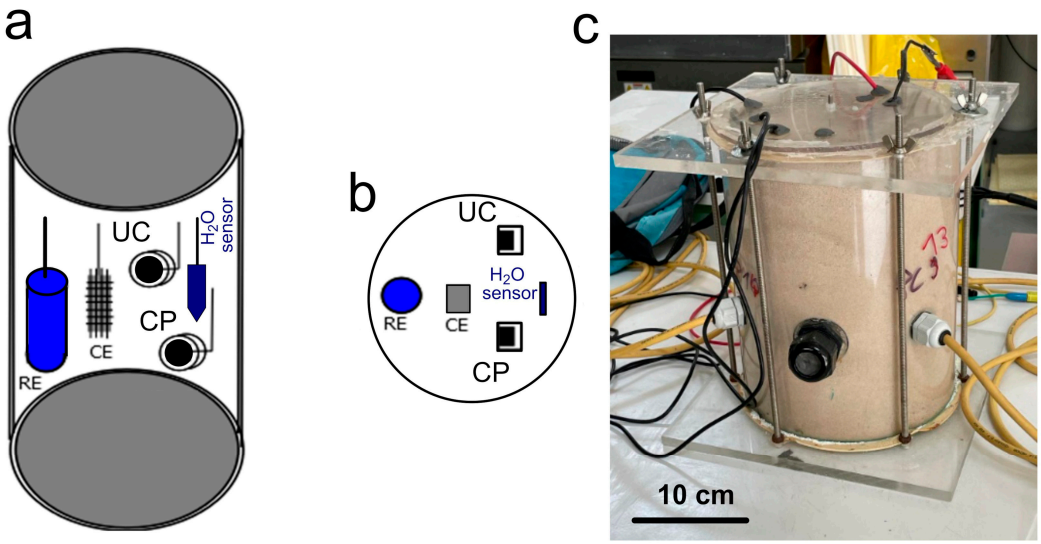

Figure 1. (**a**) Schematic representation of the cells used for the study of CP induced passivation, (**b**) top view showing the respective positions of electrodes and sensor, and (**c**) photo of an actual cell. CE = counter electrode, RE = reference electrode, UC = unprotected coupon, and CP = coupon protected by CP.

The working electrodes were disks with an active area of 1 cm^2, sandblasted before the experiments, and were set in a sample holder that allows for combining electrochemical analysis with weight loss measurements. However, the coupons underwent localization corrosion and optical microscopy was considered instead of weight loss measurements to evaluate the severity of the corrosion damage (see Section 2.4). This 1 cm^2 area is the nominal electrode surface, which is necessarily larger than the wet area, i.e., the part of the electrode actually in contact with the liquid phase. However, the current density is given in each case considering the whole surface of 1 cm^2.

The artificial soil was composed of 100% fine Fontainebleau sand NE34 (Sibelco France, Saint-Pierre-Lès-Nemours, France), with an average particle size of D_{50} = 210 µm, mainly composed of SiO_2 (99.87 wt.%). It was wetted with a solution of 0.07 M $Na_2SO_4 \cdot 10H_2O$ (97% min. purity, Sigma-Aldrich, Merck KGaA, Darmstadt, Germany) solution to obtain a soil moisture corresponding to 55% of the saturation level. This solution was chosen so that the formation of a calcareous deposit was not possible and so that localized corrosion, e.g., pitting, was not favored.

Once all of the components were set in the soil, the cell was almost completely filled, with only 2–3 cm of air left between the soil surface and the lid of the cell. It was then hermetically closed so that the soil moisture could remain constant all along the two-month experiments. Soil moisture was checked every 3 days using a Waterscout SM100 sensor (Spectrum Technologies Inc., Aurora, IL, USA). This sensor consists of two electrodes that function as a capacitor and the surrounding soil as the dielectric. An 80 MHz oscillator drives the capacitor, and a signal proportional to the soil dielectric permittivity is recorded. The dielectric permittivity of water is much greater than that of air, soil minerals, and organic matter, so changes in water content can be correlated to soil moisture. The sensor was buried in the soil at the same level as the steel electrodes and was connected to the soil moisture sensor reader each time a measurement had to be carried out. These measurements showed that soil moisture actually remained between 50% and 55% of saturation all along the experiments.

2.2. Methodology

Two series of experiments were carried out. In the first series, the protected electrode, called CP1, was successively polarized at three decreasing E_{CP} values (corrected from the ohmic drop), i.e., -0.75 V/Cu-$CuSO_4$ for 20 days, -0.94 V/Cu-$CuSO_4$ for 14 days, and -1.13 V/Cu-$CuSO_4$ for 15 days, thus defining three sequences. Each sequence ended with an interruption of CP during which the behavior of the electrode was monitored over time via OCP measurements. Additionally, LPR and EIS measurements were performed 24 h after CP was stopped to obtain more accurate information about the passive state possibly induced by the previously applied CP. After a variable time that depended on the observed behavior of the electrode, the cathodic polarization was applied again, set at the next E_{CP} value, and so on until the end of the experiment, after 57 days.

In the second series of experiments, the protected electrode, called CP2, was permanently polarized at $E_{CP} = -0.6$ V/Cu-$CuSO_4$ during 56 days. This corresponds, with respect to the EN ISO 15589-1:2017 standard [1], to an insufficient protection, even if this E_{CP} value is significantly lower (about 100 mV) than the OCP of steel buried in the same condition (see Section 3.1). During this period, voltammetry was used at days 4, 7, 14, 28, and 42 to follow the behavior of electrode CP2, and, in particular, to determine the value of the corrosion potential E_{cor}. After 56 days, CP was stopped and the behavior of electrode CP2 was studied via OCP, EIS, and LPR, as previously described for coupon CP1.

The behavior of the unprotected electrodes, called UC1 and UC2, buried together with the protected electrodes in both series of experiments, was studied using OCP, LPR, and EIS. The UC coupons were only used as reference coupons to describe the state of the metal without CP, being both the initial state of the metal and its evolution over time in the absence of CP. All of the UC electrodes behave similarly, and electrode UC1, buried with CP1, was chosen as an example for the description of the obtained results.

2.3. Electrochemical Methods

All electrochemical measurements were carried out with a Gamry1000 potentiostat (Gamry Instruments, Warminster, PA, USA) and the data acquired using the associated Framework V4.35 software.

EIS was used to determine the soil electrolyte resistance R_s, a parameter that can be determined from a Nyquist (or Bode) representation of the EIS data without any modeling [4,23]. The determination of R_s is necessary to correct the electrode potential from the ohmic drop, which is achieved using the following expression:

$$E_{IRfree} = E - I \times R_s \quad (1)$$

where E_{IRfree} is the corrected potential, E is the applied potential, R_s is the soil electrolyte resistance, and I is the current flowing through the electrode. The given value of the protection potential, E_{CP}, is, in any case, corrected from the ohmic drop. Its value fluctuated slightly around the targeted value because I and R_s varied with time. Correction of the

ohmic drop was then performed each day to adapt the value of the applied potential E to the newly measured values of I and R_s.

The R_s value was also used to monitor the evolution of the wet area of the electrode over time and to study its link with the protection potential E_{CP}.

For these EIS measurements that focused on the determination of R_s, only the high frequency range was investigated, from 100 kHz to 100 Hz, with 10 points per decade. The AC voltage perturbation amplitude, applied whether at E_{CP} for protected steel electrodes or at OCP for unprotected electrodes and protected electrodes during the interruptions of CP, was set at 20 mV rms because of the important ohmic drop characteristics of unsaturated soils.

For LPR carried out on unprotected electrodes and on protected electrodes during the interruptions of CP, the potential was varied on a range of ±30 mV around OCP, with a scan rate of $dE/dt = 0.1$ mV/s. The R_p value was determined from the slope of the obtained E vs. I curve, denoted R_p', and from the soil electrolyte resistance R_s determined using EIS, using the following expression:

$$R_p = R_p' - R_s \quad (2)$$

Voltammetry was finally carried out to study the behavior of electrode CP2, and, in particular, to determine the evolution of its corrosion potential E_{cor} over time. The polarization curves were recorded at a scan rate of $dE/dt = 0.2$ mV/s from the protection potential E_{CP}, i.e., about −0.6 V/Cu-$CuSO_4$, up to E_{IRfree} = −0.25 V/Cu-$CuSO_4$. The potential of the electrode was then set back at E_{CP}.

2.4. Surface Analysis

XRD was used to characterize the corrosion products present on the surface of the electrodes after the experiments. This analysis was carried out using an Inel EQUINOX 6000 diffractometer (Thermo Fisher Scientific, Waltham, MA, USA) with Co-Kα radiation (λ = 0.17903 nm). This system is equipped with a CPS 590 detector that collects the diffracted photons in a 2θ range of 90°. The XRD pattern was acquired during 45 min with a constant angle of incidence of 5°. Phases were identified via the ICDD-JCPDS (International Center for Diffraction Data—Joint Committee on Powder Diffraction Standards) PDF2 database, and the diffraction peaks were indexed according to the corresponding files.

Once they were characterized using XRD, the corrosion product layers were removed from the steel electrodes according to the NF-ISO 8407:2010 standard [32], i.e., using a solution of hydrochloric acid (HCl) and hexamethylenetetramine. Visual observation revealed that the electrodes suffered localized corrosion in any case, and an OM analysis was then carried out to quantify the corrosion depth using a LEICA DM 6000 M optical microscope (LEICA Microsystems GnbH, Wetzlar, Germany).

3. Results

3.1. Corrosion Behavior of Unprotected Carbon Steel Coupons

Figure 2 displays the evolution over time of OCP, soil electrolyte resistance R_s measured using EIS, and polarization resistance R_p determined from LPR of coupon UC1. First, it can be seen that the OCP remained approximately constant, measured, in any case, between −0.48 and −0.54 V/Cu-$CuSO_4$. In contrast, R_p continuously increased over time from 2350 Ω cm^2 after 1 day to 9600 Ω cm^2 at the end of the experiment. This increase in R_p corresponds to a decrease in corrosion rate, a commonly observed trend that is generally attributed to the formation and thickening of the corrosion product layer. However, the increase in R_p is associated with a significant increase in R_s. Actually, R_s increased from 1750 Ω cm^2 after 1 day to 5650 Ω cm^2 at the end of the experiment, i.e., R_s had more than tripled during the experiment. This simultaneous increase in both R_p and R_s was observed in any case and cannot be interpreted, for instance, as a fortuitous local drying of the soil at the vicinity of coupon UC1, a local drying which indeed could have led to an increase of R_s [23,24,26]. The increase in R_s is associated with the increase in R_p, and hence with the growth of the corrosion product layer that forms in the corroding areas of the metal. The reasons for this evolution are not yet known and would require further investigation.

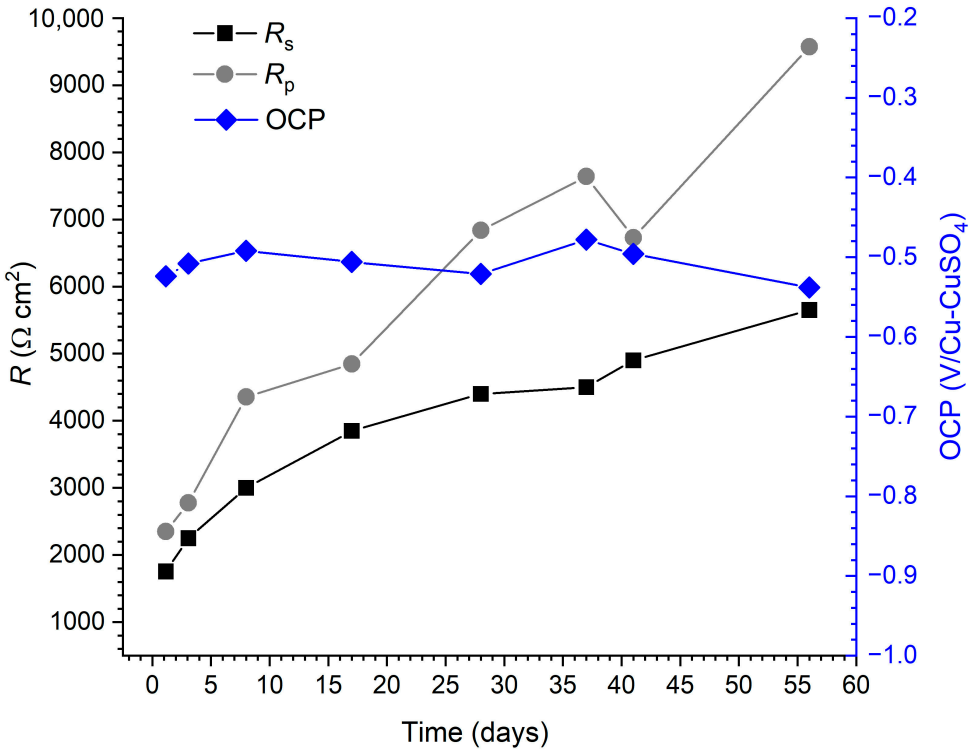

Figure 2. OCP, R_p, and R_s vs. time curves obtained for coupon UC1, i.e., the unprotected coupon buried together with coupon CP1. The accuracy of OCP measurements is ±1 mV, and the accuracy on both R_s and R_p values is ±5%.

3.2. Evolution of Carbon Steel Coupon CP1 with Decreasing Applied Potentials

The initial R_s value measured for coupon CP1 was 1500 Ω cm^2, i.e., similar to that measured for coupon UC1 at the beginning of the experiment (1750 Ω cm^2, see Figure 2). The initial OCP value of CP1 was really close to that of coupon UC1, with only a 4 mV difference. This shows that coupons UC1 and CP1 were initially set in very similar soil environments and conditions.

After 2 h at OCP, coupon CP1 was polarized at −0.745 ± 0.005 V/Cu-CuSO$_4$ for 20 days. CP was then interrupted for 3 days, and the second CP sequence then began. Table 1 gathers the information related to each CP sequence. The applied potential was decreased after each sequence, i.e., was equal to −0.935 V/Cu-CuSO$_4$ during sequence 2 and −1.13 V/Cu-CuSO$_4$ during sequence 3.

Table 1. Characteristic features of each CP sequence applied to coupon CP1: duration of the CP period and subsequent interruption period, average applied potential (E_{CP}, corrected from the ohmic drop), average cathodic protection current density (j_{CP}), and R_s value reached at the end of each CP application period. The accuracy on R_s values is ±5%.

	CP Sequence 1	**CP Sequence 2**	**CP Sequence 3**
CP application period	Day 0 to day 20	Day 23 to day 37	Day 41 to day 56
E_{CP} (V/Cu-CuSO$_4$)	−0.745 ± 0.005	−0.935 ± 0.01	−1.13 ± 0.02
j_{CP} (mA cm^{-2})	−0.24 ± 0.02	−0.77 ± 0.01	−2.45 ± 0.15
R_s (Ω cm^2)	750 (day 17)	450 (day 36)	330 (day 55)
Interruption of CP	Day 20 to day 23	Day 37 to day 41	Day 56 to day 57 (end)

The first consequence of the decrease in applied potential is an increase in the cathodic current density j_{CP} (in absolute value). $|j_{CP}|$ increased from 0.24 mA cm^{-2} for E_{CP} = −0.745 V/Cu-CuSO$_4$ to 2.45 mA cm^{-2} for E_{CP} = −1.13 V/Cu-CuSO$_4$. Decreasing the potential increases the cathodic reaction rate, and hence increases $|j_{CP}|$.

However, the cathodic polarization induced other effects, as demonstrated by the decrease of R_s due to CP. R_s decreased from 1500 Ω cm^2 before CP was applied to 750 Ω cm^2 when the coupon was polarized at E_{CP} = −0.745 V/Cu-CuSO$_4$. Moreover, the lower the E_{CP}, the lower the R_s, so that R_s reached 330 Ω cm^2 for the lowest applied potential of −1.13 V/Cu-CuSO$_4$. This decrease in R_s because of CP was already reported [4,5]. It can result from electrocapillary effects that modify the liquid/solid contact angle at the gas/liquid/solid boundary and lead to a spreading of the liquid phase on the steel surface [27–30]. This spreading of the electrolyte increases the wet area and thus decreases R_s. This is only possible in unsaturated soil conditions where the pores of the soil are partially filled with air, which is the case in the experimental conditions considered here. The decrease in R_s can also result from an increase in electrolyte conductivity. The cathodic polarization increases the cathodic reaction rate and thus the production of OH^- ions, whether the reaction is an O_2 reduction (3) or a H_2O reduction (4), as follows:

$$O_2 + 2H_2O + 4e^- \rightarrow 4OH^- \quad (3)$$

$$2H_2O + 2e^- \rightarrow H_2 + 2OH^- \quad (4)$$

The massive production of OH^- ions at the steel/soil interface activates the migration of cations (mainly Na^+ in our experimental conditions) so that the conductivity of the electrolyte at the vicinity of the steel surface is necessarily increased. Note that, of course, the production of OH^- ions increases the pH at the steel/soil interface.

3.3. CP-Induced Passivation of Carbon Steel Coupon CP1

The same phenomenon was observed for each interruption of CP. The interruption following the second CP sequence was considered as an example. Figure 3 displays the evolution of the OCP of coupon CP1 during this interruption, which lasted 102 h from day 37 to day 41.

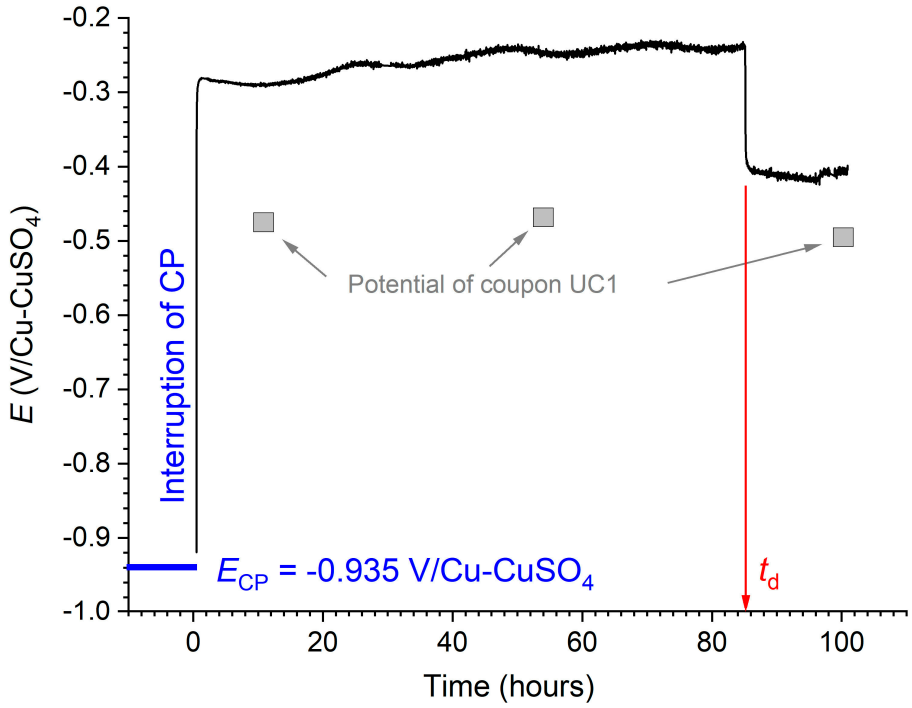

Figure 3. OCP vs. time curve (black line) obtained for coupon CP1 after the second CP sequence. The OCP of unprotected coupon UC1, measured every two days, is displayed as gray squares. The blue line corresponds to the potential applied to coupon CP1 before the interruption of CP, i.e., E_{CP} = −0.935 V/Cu-CuSO$_4$. Time 0 corresponds to the moment when CP was stopped.

Figure 3 shows that the OCP of coupon CP1 increased rapidly as soon as CP was stopped. It reached –0.285 V/Cu-$CuSO_4$ after 1.3 h and remained approximately constant during 12 h. It tended to increase slightly over time, with slight periodic oscillations. The period of these oscillations is 24 h, and it can be put forward that the periodic variation in OCP is due to changes in temperature associated with the day/night cycles. The OCP reached a maximum of −0.234 V/Cu-$CuSO_4$ after 85.2 h, a time denoted t_d. The OCP then dropped to a smaller value around −0.41 V/Cu-$CuSO_4$. This value is similar to that of the unprotected coupon UC1, measured at an average value of −0.48 V/Cu-$CuSO_4$ at that time (Figure 3, gray squares).

The OCP drop of about 0.18 V observed at time t_d is similar to a passive to active transition. This phenomenon was already reported, and it was observed that the re-activation of the steel surface was due to the decrease in pH at the steel/soil interface and corresponded to a localized corrosion process [9]. This conclusion implies that the steel surface was in a passive state before time t_d. This would explain the high OCP value observed for coupon CP1 with respect to coupon UC1.

To validate this assumption, EIS and LPR were performed on coupon CP1 before (i.e., 24 h after the interruption of CP) and after time t_d. R_p was determined to be as high as 45,000 Ω cm^2 before t_d. It dropped to 6500 Ω cm^2 after t_d. This drop in R_p, associated with the drop in OCP, confirms that the phenomenon occurring at t_d is a passive to active transition. Time t_d is then the time before depassivation occurs, i.e., the time during which the steel surface remains passive.

EIS measurements performed before t_d demonstrated that R_s increased because of the interruption of CP. It reached 1650 Ω cm^2 after 24 h while it was equal to 450 Ω cm^2 when CP was applied (Table 1).

Finally, Figure 4 shows typical LPR and EIS results. Figure 4a displays the polarization curves used for the determination of R_p obtained before (day 38) and after (day 41) depassivation. The drop in R_p after depassivation (i.e., after time t_d) is clearly illustrated by the increase in the slope of the $j(E)$ curve. Figure 4b shows the EIS results obtained after the interruption of CP at days 37, 38, and 41, displayed as modulus of Z vs. log(frequency). This representation was chosen as it clearly illustrates the increase in R_s observed after CP was interrupted. In the small frequency range considered for the present study, the modulus of the impedance increases very slightly with decreasing frequency. The R_s value can be measured at the highest frequencies (typically 10 kHz).

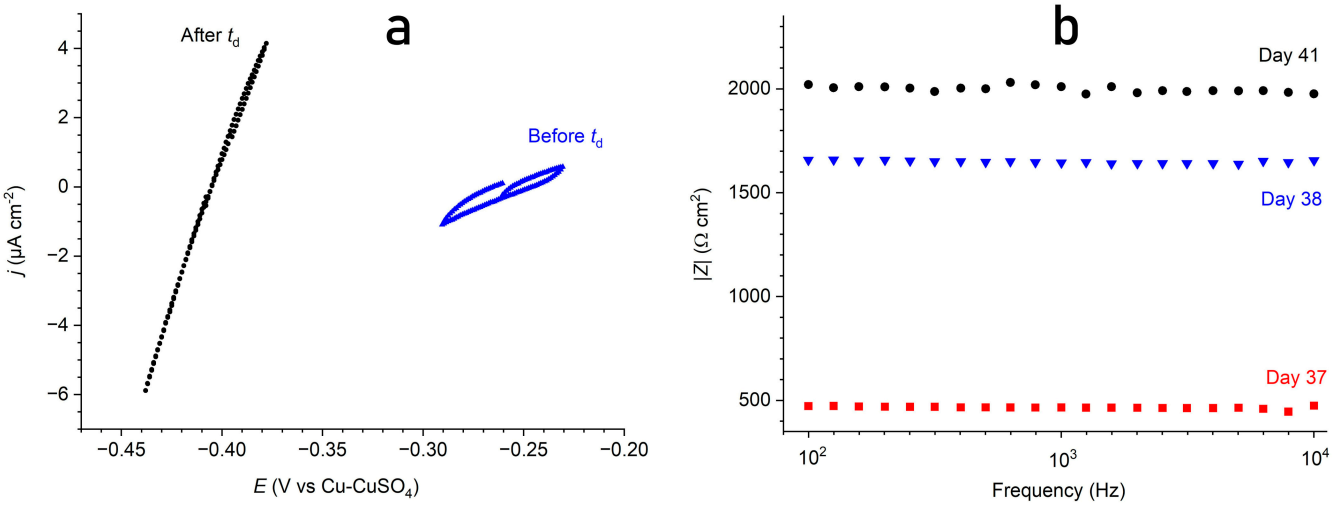

Figure 4. LPR and EIS results obtained for coupon CP1 during the second interruption of CP: (**a**) LPR curves $j(E)$ obtained before (day 38, in blue) and after (day 41, in black) depassivation; E is the applied potential not corrected from the ohmic drop, and (**b**) $|Z|$ vs. log(frequency) curves obtained at days 37 (red squares), 38 (blue triangles), and 41 (black dots). The data obtained at frequencies higher than 10 kHz are in most cases noisy, and were not displayed for the sake of clarity.

Similar results were obtained during the interruptions of CP after CP sequences 1 and 3 (note, however, that the experiment was stopped before depassivation of the steel surface after CP sequence 3). Both R_p and R_s values measured 24 h after the interruption of CP seem to depend on the previous CP period. To illustrate this point, the results obtained after CP sequence 3 can be compared to those described above, obtained after sequence 2. After CP sequence 3, R_p was measured at 36,000 Ω cm^2, i.e., was lower than that measured after sequence 2. However, R_s was also smaller, equal to 750 Ω cm^2.

The increase in R_s observed once CP is interrupted (see Figure 4b) indicate that the wet area decreases. A decrease in wet area, i.e., a decrease in the fraction of the surface that is electrochemically active, necessarily induces an (apparent) increase in R_p. Therefore, any variation of R_p can be due, at least partially, to a variation of wet area. The interpretation of changes in R_p must then take into account the associated changes in R_s, which can be achieved considering the changes in the R_p/R_s ratio.

The R_p/R_s ratio for the passive state induced by CP at −1.13 V/Cu-CuSO$_4$ (sequence 3), equal to 48.0, is higher than the R_p/R_s ratio for the passive state induced by CP at −0.935 V/Cu-CuSO$_4$ (sequence 2), equal to 27.3. This may indicate that the passive layer induced by CP at −1.13 V/Cu-CuSO$_4$ was more protective than the passive layer induced by CP at −0.935 V/Cu-CuSO$_4$.

3.4. Monitoring and CP-Induced Passivation of Carbon Steel Coupon CP2

For coupon CP2 polarized at E_{CP} = −0.60 V/Cu-CuSO$_4$ for 56 days, voltammetry was used to monitor the evolution over time of the corrosion potential of the electrode. This evolution is displayed in Figure 5, together with that of R_s. Values computed for E_{CP} using Equation (1) are also given to show that E_{CP} remained close to the targeted value of −0.60 V/Cu-CuSO$_4$, i.e., remained comprised between −0.610 V/Cu-CuSO$_4$ and −0.583 V/Cu-CuSO$_4$. The polarization curves used to determine E_{cor} at days 4, 7, 14, and 42 are presented in Figure 6.

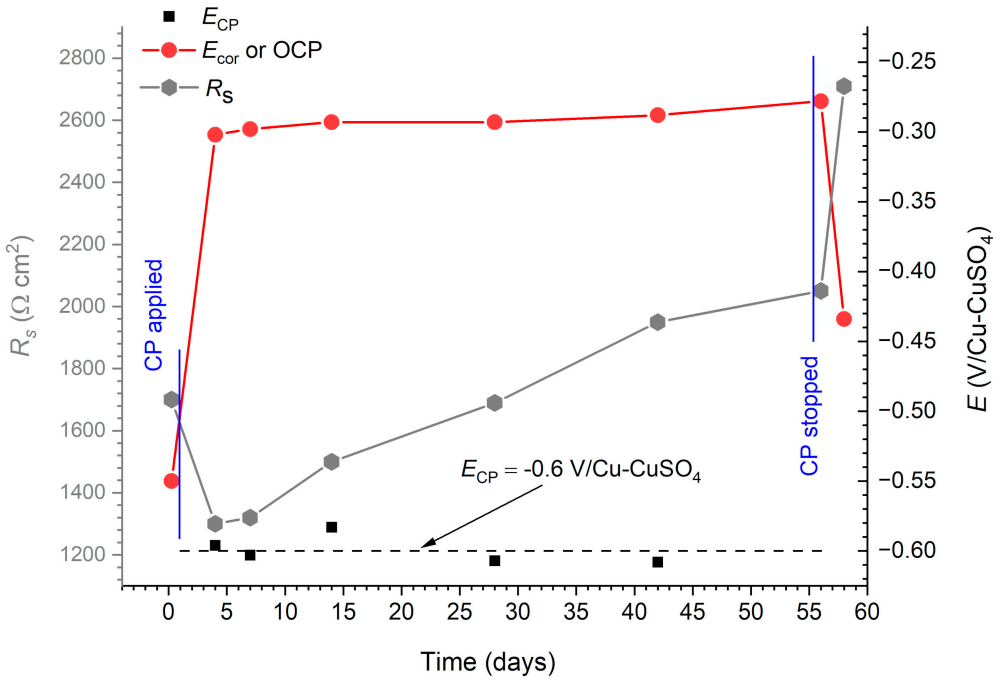

Figure 5. Evolution over time of R_s (gray curve and hexagons), E_{CP} (black dotted line and squares), and E_{cor}/OCP (red curve and circles) for coupon CP2. CP was applied from t = 2 h to t = 56 days.

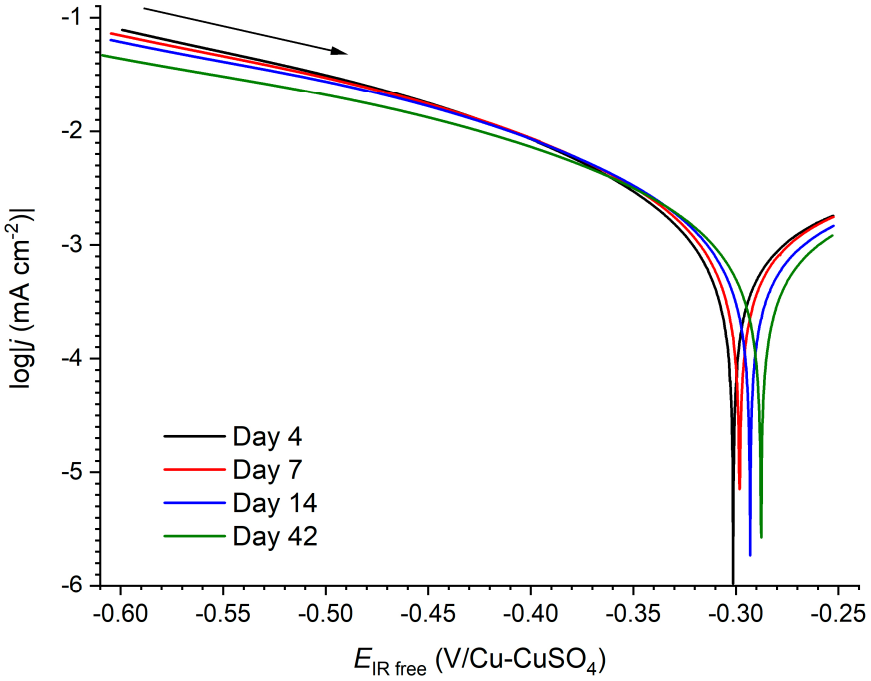

Figure 6. Polarization curves of coupon CP2 obtained at days 4 (black line), 7 (red line), 14 (blue line), and 42 (green line). The polarization curve obtained at day 28 was omitted for clarity. The arrow indicates the direction of the potential scan.

In the following paragraphs, it is assumed, for simplification, that OCP and E_{cor} are equivalent, which is the case in theory. In practice, E_{cor} may slightly differ from OCP, particularly because of the charging current associated with capacitive effects [33].

Figure 5 shows that the application of CP, as for coupon CP1, induced a decrease of R_s from 1700 Ω cm^2 before CP was applied to 1300 Ω cm^2 at day 4. This decrease is less important than those induced by the stronger cathodic polarization potentials applied to coupon CP1, which confirms that, in our experimental conditions, the lower the applied potential, the smaller the R_s. Moreover, R_s increased with time, as observed for the unprotected coupons (see Figure 2, coupon UC1). It remained significantly smaller than that of unprotected coupons, reaching 1950 Ω cm^2 at day 42, while it was measured at about 5000 Ω cm^2 for the unprotected coupons the same day.

The application of CP also rapidly induced an increase in the corrosion potential. E_{cor} increased from the initial OCP value of −0.550 V/Cu-CuSO$_4$ to −0.302 V/Cu-CuSO$_4$ after 4 days of CP. It increased only slightly afterwards to reach −0.288 V/Cu-CuSO$_4$ at day 42. The four polarization curves of Figure 6 are similar and confirm that the system did not change significantly between day 4 and day 42. The slight increase in E_{cor} with time is clearly visible, too. The polarization curves also show that O_2 reduction is not controlled by diffusion, or only partially far from OCP. The experimental soil conditions considered here are far from saturation (50–55% sat.), and thus the transport of O_2 is facilitated, as it mainly takes place in the gas phase, partially filling the pores of the soil. Similar conclusions were already reported [9].

Finally, when the cathodic polarization of coupon CP2 was stopped, the OCP increased rapidly to reach −0.278 V/Cu-CuSO$_4$, i.e., a value similar to that measured for E_{cor} using voltammetry. The experiment was stopped at day 58 after the depassivation of coupon CP2. The OCP had dropped to −0.434 V/Cu-CuSO$_4$, while R_s increased up to 2710 Ω cm^2.

Figure 7 more precisely shows the evolution over time of the OCP of coupon CP2 once CP was stopped. This curve is really similar to that of coupon CP1 (Figure 3), but is actually shorter because the depassivation took place earlier at t_d = 37.6 h. The polarization resistance of coupon CP2 was measured 24 h after the interruption of CP and was found

to be as high as 35,000 Ω cm^2. It was also measured after t_d and was observed to have dropped to 4000 Ω cm^2.

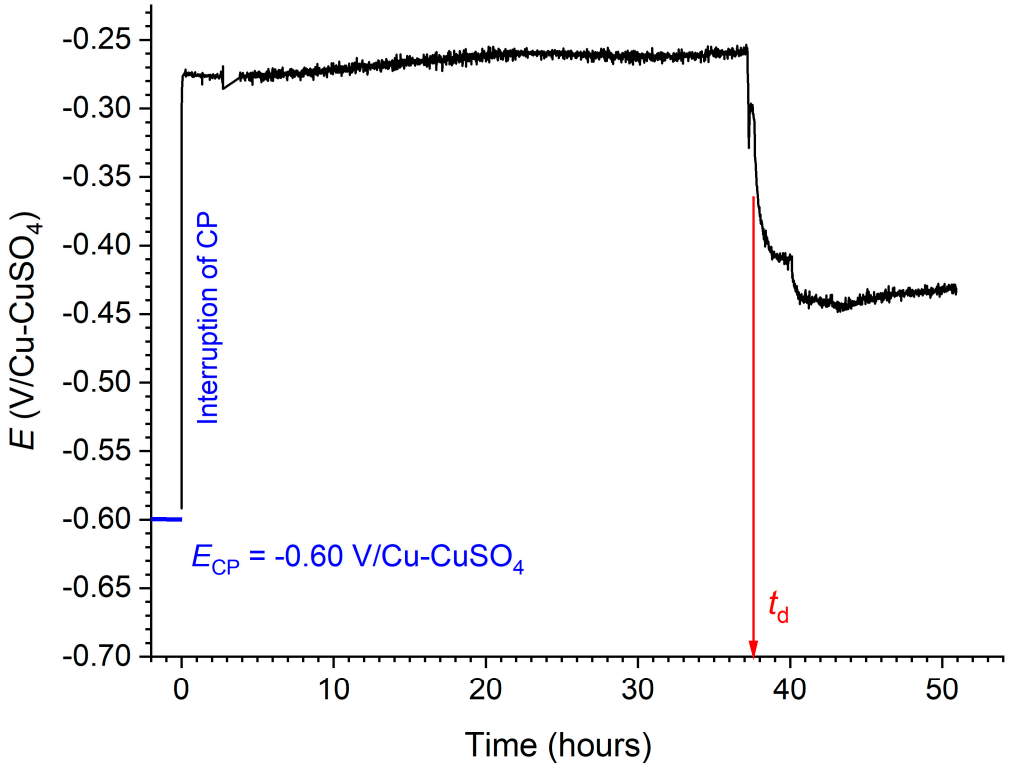

Figure 7. OCP vs. time curve (black line) obtained for coupon CP2 after CP was stopped. The blue line corresponds to the potential applied before the interruption of CP, i.e., $E_{CP} = -0.60$ V/Cu-CuSO$_4$. Time 0 corresponds to the moment when CP was stopped.

3.5. Observation and Analysis of the Steel Coupons

The soil was removed as gently as possible from the steel surface so that the morphology of the corrosion product layer could be observed. However, the soil covering the unprotected coupons was colored in brown by rust as far as 3 mm from the steel surface. This zone, where the soil is mixed with corrosion products, is a transient region, sometimes called a transformed medium [34], between the corrosion product layer and the soil sensu stricto. The transformed medium then had to be removed so that the steel surface could be observed, which was achieved for coupon UC1, but not for coupon UC2.

Figure 8 displays the images of the surface of coupons UC1 and CP1 once the soil and the transformed medium were removed (Figure 8a,b). They are compared to the images obtained after the removal of the corrosion products (Figure 8c,d).

Figure 8a,c clearly show that only a small part of coupon UC1 was actually corroded while the rest of the surface appeared undamaged. These images are consistent with EIS measurements: the wet area corresponds to the corroded surface, i.e., the surface covered by brown corrosion products in Figure 8a, and the wet area was only a small fraction of the overall surface of the electrode, hence leading to high R_s values. More precisely, it has been proposed recently [26] that the main central part of a "wet area" was an anodic zone, while its periphery was a cathodic zone. In unsaturated soil, O_2 is mainly transported in the gas phase and subsequently dissolves in the electrolyte close to the metal surface, more likely at the vicinity of the triple-phase boundary, i.e., the gas/electrolyte/metal boundary. Therefore, in Figure 8c, the corroded zones (broad pits) may correspond to the anodic regions of the wet areas, while a small region of the surrounding metal may have been in contact with the liquid phase and act as a cathodic zone. The growing corrosion products may progressively cover this cathodic area, thus decreasing the cathodic reaction rate and

hence the corrosion rate. Comparing Figure 8a,c, it can be seen that the areas covered with rust are slightly larger than the corresponding broad pits.

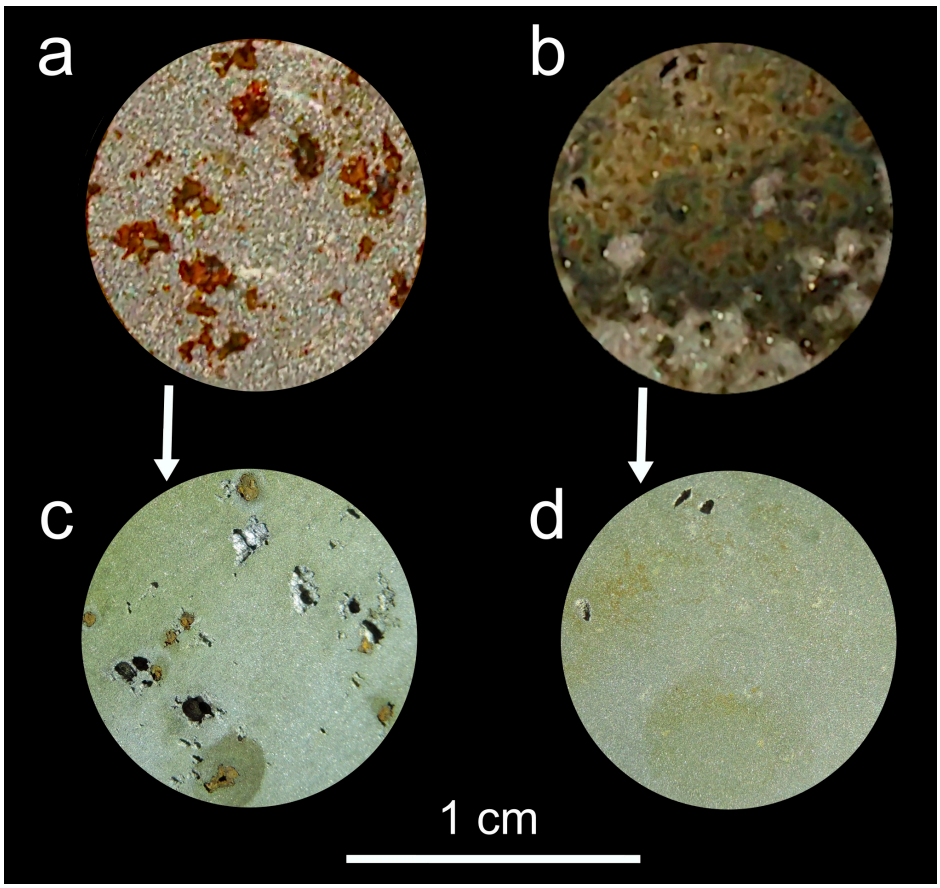

Figure 8. Images showing the surface of coupons UC1 (**a**,**c**) and CP1 (**b**,**d**) at the end of the experiment. Images (**a**,**b**) were obtained before the removal of the corrosion products, while images (**c**,**d**) were obtained after the removal of the corrosion products.

Conversely to coupon UC1, most of the surface of coupon CP1 was covered by a thin layer (visual appreciation) of corrosion products (Figure 8c). The wet area was similar to the overall surface of the electrode, in agreement with the measured smaller R_s values. This definitively confirms that CP induced a spreading of the liquid phase on the metal surface.

Figure 8c shows numerous severe localized degradations on the surface of unprotected coupon UC1, with a maximal corrosion depth of 700 µm. In contrast, only three small pits are visible on the surface of coupon CP1 (Figure 8d). These pits result from the interruptions of CP [9], and more precisely from the depassivation process observed after CP sequences 1 and 2. The maximal depth was measured at 200 µm.

The comparison between Figure 8b,d also shows that the thin corrosion product layer covering most of the steel surface is rather protective, as the steel underneath does not seem degraded. This layer may then be responsible for the high R_p values measured after the interruptions of CP. It cannot be considered to be a passive film, which is typically 1–2 nm thick [35] and is not visible to the naked eye, and may rather be denoted as a "pseudo-passive" layer. Note, however, that the presence of a 1–2 nm thick passive layer below the visible blackish layer cannot be discarded.

The minerals present on the surface of the coupons after the experiment were characterized using XRD (Figure 9). The unprotected coupon considered here is UC2, which was left covered with a part of the transformed medium, i.e., the transition region between the corrosion products and the soil, so that the corrosion products present in the transformed medium could also be identified. Consequently, the main peaks visible in the correspond-

ing XRD pattern (Figure 9a) are those of quartz, i.e., the main mineral (99.87 wt.%) present in the considered artificial soil. Thenardite, i.e., sodium sulfate, is also detected. It results from the post-experiment evaporation of water (more likely during the XRD analysis itself), as the electrolyte was a Na_2SO_4 solution. Two corrosion products are identified, namely goethite α-FeOOH and lepidocrocite γ-FeOOH. These are typical corrosion products of steel in aerated soils [26].

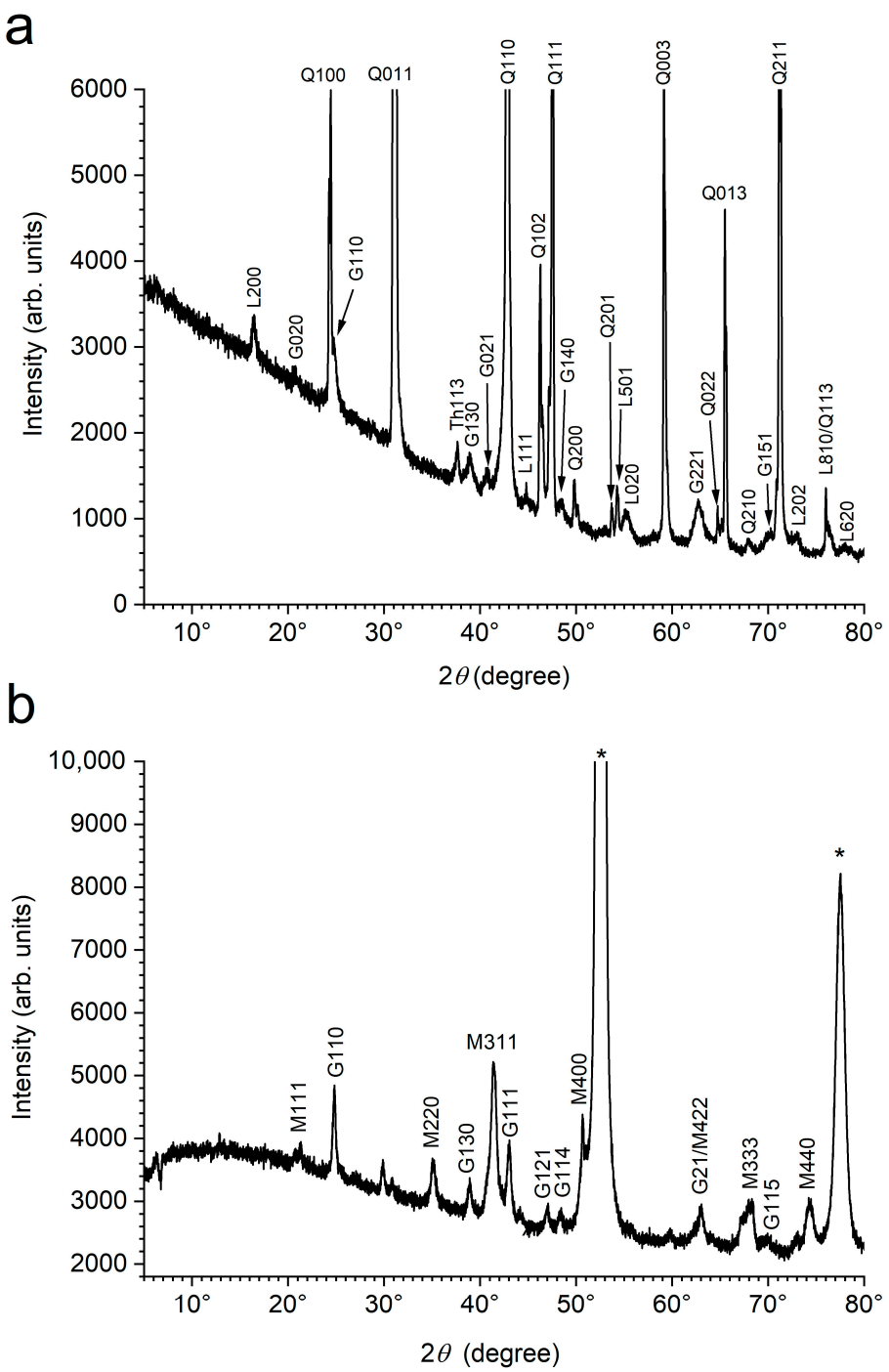

Figure 9. XRD patterns of coupons UC2 (**a**) and CP1 (**b**). G = goethite, L = lepidocrocite, M = magnetite, Q = quartz, and Th = thenardite (Na_2SO_4). The diffraction lines are denoted with the corresponding Miller index. The very intense peaks denoted by a star are those of the substrate (α-Fe).

The XRD pattern of coupon CP1 obtained after removal of the soil is displayed in Figure 9b. The main peaks, very intense, are those of the substrate, which confirms that the mineral layer is indeed very thin. This finding is consistent with the observed protective ability of this layer, which can be considered to be a pseudo-passive layer. As for UC2, goethite is present, but the main component of the pseudo-passive layer is magnetite Fe_3O_4. This finding is consistent with a previous study [17] which showed that magnetite was the most protective compound associated with CP in a 3.5% NaCl solution. It was obtained at the lowest potential (−1.3 V/Ag-AgCl-3.5% NaCl in [17], approximately –1.41 V/Cu-$CuSO_4$). It is generally considered that CP-induced passivation (or pseudo-passivation) involves an increase in the interfacial pH, and magnetite is indeed favored with respect to other Fe(II,III) mixed valence compounds, such as green rusts in alkaline conditions [36,37]. Magnetite is also favored with respect to Fe(III) compounds, such as goethite and lepidocrocite, at low potentials [37].

Figure 10 displays the images of coupon CP2 before and after the removal of corrosion products. Figure 10a reveals the presence of numerous spots of rust scattered all over the surface of the electrode. No pseudo-passive layer similar to that observed for coupon CP1 is visible on the surface of coupon CP2. A nanometric passive layer may have formed in this case.

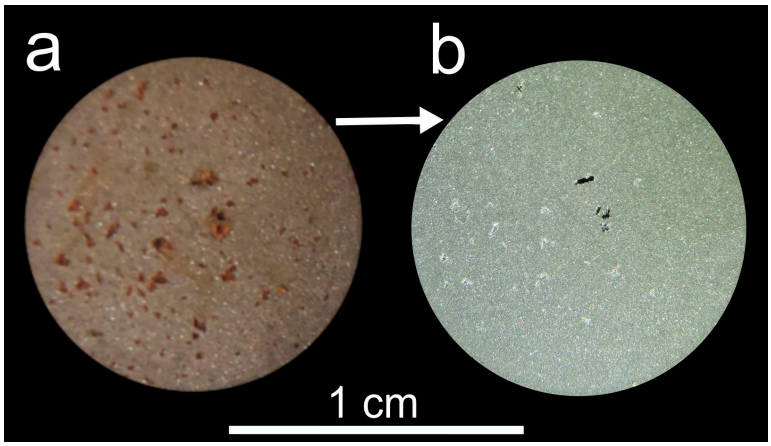

Figure 10. Images showing the surface of coupon CP2 at the end of the experiment. Image (**a**) was obtained before the removal of the corrosion products, while image (**b**) was obtained after the removal of the corrosion products.

Figure 10b shows that the metal is slightly degraded under most of the spots of rust. It can be put forward that the passive layer was rather defective, with numerous weak zones where some corrosion could have occurred even when CP was applied. Three more severe pits are, however, seen near the center of the electrode. The corrosion depth was determined using OM to be about 80–100 µm in these pits.

4. Discussion

In the experimental conditions considered here, whatever the applied cathodic potential, from −0.6 V/Cu-$CuSO_4$ (approximately OCP-100 mV) to −1.13 V/Cu-$CuSO_4$, CP-induced passivation or pseudo-passivation was observed. This shows that the increase in the interfacial pH was sufficient in each case to induce the formation of a protective oxide film. The use of voltammetry for coupon CP2 demonstrated that passivation was rapidly induced by CP. The first polarization curve, acquired after 4 days of CP, showed that E_{cor} already increased to a value typical of the passive state. The system did not change significantly afterwards, except for a slight increase in E_{cor}, which may reflect an increase in the passive film thickness [38,39].

In aerated soils, the main cathodic reaction, except for very low cathodic potentials, is oxygen reduction. The increase in pH at the steel/soil interface is then linked to the rate of

oxygen reduction, which is measured using the cathodic protection current density $|j_{CP}|$. However, it is also linked to the transport of OH^- ions from the steel surface. A moderate decrease in potential, e.g., from OCP to OCP-100 mV, necessarily increases the rate of production of OH^- ions compared to the conditions met at OCP. Our results show that the associated increase in interfacial pH was sufficient, even for this moderately cathodic potential, to induce passivation. A decrease in applied potential increases the cathodic reaction rate, i.e., the rate of production of OH^- ions at the steel surface, as testified here by the increase of $|j_{CP}|$ with decreasing E_{CP} values. This should favor the increase in interfacial pH, in agreement with the previous literature data [8,9]. However, a decrease in applied potential also strengthens the migration of OH^- ions from the steel surface, which opposes (together with diffusion) the accumulation of OH^- ions at the vicinity of the steel/soil interface. In unsaturated soil, it was shown that the diffusion and migration of OH^- ions did play a major role in the increase in interfacial pH during CP application and in its decrease after interruption of CP [9]. This was revealed through the influence of electrode size and by observing differences in pH between the center and edges of large electrodes. The pH is lower at the edges of a large electrode and lower for a smaller electrode because the transport of OH^- ions is facilitated because the ions can also diffuse away from the steel parallelly to the metal surface [9].

Table 2 gathers the information related to the passive state for the three main considered CP levels, i.e., $E_{CP} = -0.60$ V/Cu-$CuSO_4$, $E_{CP} = -0.935$ V/Cu-$CuSO_4$, and $E_{CP} = -1.13$ V/Cu-$CuSO_4$. As noted earlier, no clear trend can be identified from the R_p values because of the effects of CP on the wet area. This last point is illustrated by the link between R_s and E_{CP}: the lower the protection potential, the lower the R_s value. CP favors the spreading of the liquid phase on the steel surface [4,5] via electrocapillary effects [27–30], as clearly illustrated in Figure 8.

Table 2. CP-induced passivation: R_p and R_s values measured 24 h after the interruption of CP for the three main considered CP levels for coupons CP1 and CP2. The accuracy on both R_s and R_p values is ±5%.

	CP2	CP1 Sequence 2	CP1 Sequence 3
E_{CP} (V/Cu-$CuSO_4$)	-0.60 ± 0.02	-0.935 ± 0.01	-1.130 ± 0.02
R_p (Ω cm^2)	35,000	45,000	36,000
R_s (Ω cm^2)	2050	1650	750
R_p/R_s	17.1	27.3	48.0

However, the R_p/R_s ratio is clearly increasing when E_{CP} decreases. This indicates that the passive (or pseudo-passive) layer may be more protective at lower cathodic potentials. The similitude between the measured R_p values, about 40 kΩ cm^2 in each case, is then more likely to be fortuitous. The increase protective ability of the passive (or pseudo-passive) layer with decreasing E_{CP} may be due to the link between interfacial pH and CP potential. In principle, a decrease in cathodic potential favors the increase in interfacial pH, which favors the formation of a passive oxide film.

The images of coupons CP1 and CP2 after the experiments showed that the surfaces of the coupons were rather different (see Figures 8b and 10a). The surface of CP1 was almost completely covered by a blackish thin layer that proved mainly composed of magnetite (with goethite). The surface of coupon CP2 did not show any similar layer, suggesting that the protective layer, which was not visible, was indeed a few nm-thick passive layer. However, the surface of coupon CP2 also showed numerous spots of rust, which indicates that this layer was, however, weak and defective. This is consistent with the measured R_p value of 35,000 Ω cm^2, a rather small value for a passive state. For instance, in a borate buffer, where passivation of carbon steel can take place, R_p values were obtained between 10.1 kΩ cm^2 and 8.6 MΩ cm^2, depending on the anodic potential applied [40]. The value obtained for CP2 is of the same order of magnitude as the lowest values obtained in the borate buffer. Moreover, the R_p/R_s ratio is the lowest (Table 2), confirming that the passive

layer formed in these conditions does not protect the metal as efficiently as the protective layer formed at more cathodic potentials. It is also questionable whether the deepest degradations observed at the surface of coupon CP2 are only due to the depassivation period (only a few days) or correspond to a pitting process initiated during the application of CP and due to the weakness of this imperfect passive layer.

Coupon CP2 was polarized for 56 days at the same $E_{CP} = -0.60$ V/Cu-$CuSO_4$ value, which must be considered to be insufficient protection according to the relevant standard [1]. For this insufficient CP level considered here ($E_{CP} = -0.60$ V/Cu-$CuSO_4$), although a passive film formed, it provided an imperfect protection, and it can be put forward that this may be due to an insufficient increase in the interfacial pH.

Coupon CP1 was consecutively polarized at three different decreasing cathodic potentials, with interruptions of CP between each polarization sequence. The pseudo-passive magnetite layer may have begun to form a soon as CP was applied, thus being at $E_{CP} = -0.745$ V/Cu-$CuSO_4$, but may have only formed during the last CP sequence, i.e., at $E_{CP} = -1.13$ V/Cu-$CuSO_4$. The high R_p value of 45,000 Ω cm^2 measured after CP sequence 2 ($E_{CP} = -0.935$ V/Cu-$CuSO_4$) may then be due whether to a nm-thick passive film or to the magnetite layer itself. The magnetite layer, which was necessarily present at the end of CP sequence 3, has contributed to the large R_p value measured after CP sequence 3, i.e., 36,000 Ω cm^2. The average R_p value observed here for the passive or pseudo-passive state induced by CP is about 40 kΩ cm^2. From this value, a rough estimate of the associated corrosion rate can be obtained using the Stern–Geary equation [41] with a Stern–Geary coefficient $B = 0.022$ V [42]. The computed corrosion current density is 0.5 μA cm^{-2}, which leads to a corrosion rate of steel about 6 μm yr^{-1}. The CP-induced passive (or pseudo-passive) state observed in the specific experimental conditions considered here fulfills the efficiency requirement specified in the EN ISO 15589-1:2017 standard [1], i.e., leads to a residual corrosion rate lower than 10 μm yr^{-1}.

Finally, in any case, the passive state persisted for a time t_d before depassivation and pitting occurred. In their previous thorough study of the phenomenon, Wang et al. [9] demonstrated that this depassivation was facilitated for small electrodes (smaller time t_d) and at the edges of large electrodes because of the increased OH^- diffusion at the periphery of the electrode, which promoted a faster pH decrease in this region and thus a localized weakening and breakdown of the passive layer. Our results also showed that, in unsaturated conditions, the interruption of CP was followed by a fast increase in R_s, i.e., a fast decrease in the wet area. This indicates that the electrolyte, spread on the steel surface during the application of CP, returned rapidly to a dispersed state, hence forming isolated small wet areas on the steel surface. As shown in Figure 4b, R_s had increased from 450 Ω cm^2 to 1970 Ω cm^2 when depassivation took place. The depassivation and subsequent corrosion process could then only be localized at the wet areas remaining on the electrode surface, like the corrosion process taking place on unprotected coupons (Figure 8a,c). Depassivation would then occur earlier at the wet areas located close to the periphery of the electrode, which is clearly the case for coupon CP1 as revealed by Figure 8d.

Coupon CP1 was subjected to successive CP and depassivation sequences. The depth of the three observed deep pits is important (~200 μm), and only three pits are visible, which suggests that the successive interruptions of CP could have cumulative effects, the depassivation occurring more easily in the previously created pits. It is indeed questionable whether the depassivation observed after the second CP-sequence took place in the pits previously formed after the first depassivation. The surface inside the pits may have repassivated once CP was applied again, but the pits may constitute a weak zone during the next interruption of CP. Moreover, the time required for the repassivation of the metal inside the pits is not known either, so is it is not possible to even estimate any reliable corrosion rate from the measured pit depths.

Time t_d is linked to the previously applied protection potential, as clearly illustrated by the difference between CP2 (−0.6 V/Cu-$CuSO_4$ and t_d = 37.6 h) and CP1—sequence 2

(-0.935 V/Cu-$CuSO_4$ and t_d = 85.2 h). However, it seems to depend, also, on the duration of the previous period of CP. For sequence 1 of CP1, the depassivation occurred after t_d = 35.5 h, i.e., a shorter time than that measured for CP2, while the applied potential was lower. However, CP was applied for only 20 days, while it was applied for 56 days for CP2. The thorough understanding of both effects of time and applied potential requires further study, although it can be suggested that the interfacial pH reached after the application of CP may play the major role [9].

5. Conclusions

This preliminary study of CP-induced passivation confirmed the important role of this phenomenon in the protection of buried carbon steel structures.

In the considered experimental conditions, i.e., using an artificial soil only composed of siliceous fine sand wetted at 50–55% sat. with a 0.07 M Na_2SO_4 solution, CP induced the formation of a passive or pseudo-passive oxide film. This phenomenon was observed, whatever the applied cathodic potential, from -0.6 V/Cu-$CuSO_4$ to -1.13 V/Cu-$CuSO_4$. The passive state persisted for at least 35.5 h and could then be evidenced using OCP and LPR carried out after CP was stopped. Depassivation occurred after a variable time (t_d, measured here between 35 and 85 h), leading to a localized corrosion process, in agreement with previous work [9].

The average R_p value of carbon steel in the CP-induced passive (or pseudo-passive) state, about 40 kΩ cm^2 in the experimental conditions considered for the present study, corresponds to a residual corrosion rate smaller than 10 µm yr^{-1} (estimated at ≈6 µm yr^{-1}), i.e., the specified threshold value defining an efficient CP according to the relevant standard [1]. However, the imperfect passive state that was reached in insufficient CP conditions (-0.6 V/Cu-$CuSO_4$) may favor a localized degradation of the steel surface.

Author Contributions: Conceptualization, E.F., S.F. and P.R.; methodology, E.F., M.J. and P.R.; validation, E.F., S.F., F.R. and P.R.; formal analysis, M.J. and P.R.; investigation, M.J. and P.R.; resources, E.F., M.J. and P.R.; data curation, P.R.; writing—original draft preparation, P.R.; writing—review and editing, F.R., S.F. and P.R.; visualization, P.R.; supervision, E.F. and P.R.; project administration, E.F.; funding acquisition, S.F. All authors have read and agreed to the published version of the manuscript.

Funding: This research received no external funding.

Data Availability Statement: The data that support the findings of this study are available in "figshare" with the identifier doi: 10.6084/m9.figshare.26879245.

Conflicts of Interest: Author Sylvain Fontaine was employed by the company GRTgaz. The remaining authors declare that the research was conducted in the absence of any commercial or financial relationships that could be construed as a potential conflict of interest.

References

1. *EN ISO 15589-1:2017*; Petroleum, Petrochemical and Natural Gas Industries—Cathodic Protection of Pipeline Systems—Part 1: On-Land Pipelines. International Organization for Standardization (ISO): Geneva, Switzerland, 2017; pp. 8–9.
2. Barbalat, M.; Lanarde, L.; Caron, D.; Meyer, M.; Vittonato, J.; Castillon, F.; Fontaine, S.; Refait, P. Electrochemical determination of residual corrosion rates of steel under cathodic protection in soils. *Corros. Sci.* **2012**, *55*, 246–253. [CrossRef]
3. Barbalat, M.; Caron, D.; Lanarde, L.; Meyer, M.; Fontaine, S.; Castillon, F.; Vittonato, J.; Refait, P. Estimation of residual corrosion rates of steel under cathodic protection in soils via voltammetry. *Corros. Sci.* **2013**, *73*, 222–229. [CrossRef]
4. Nguyen, D.D.; Lanarde, L.; Jeannin, M.; Sabot, R.; Refait, P. Influence of soil moisture on the residual corrosion rates of buried carbon steel structures under cathodic protection. *Electrochim. Acta* **2015**, *176*, 1410–1419. [CrossRef]
5. Nguyen, D.D.; Jeannin, M.; Sabot, R.; Fleury, E.; Refait, P. On the use of voltammetry to estimate the efficiency of cathodic protection of buried steel structures. *J. Mater. Eng. Perform.* **2019**, *28*, 6042–6052.
6. Mahlobo, M.G.R.; Olubambi, P.A.; Mjwana, P.; Jeannin, M.; Refait, P. Study of overprotective-polarization of steel subjected to cathodic protection in unsaturated soil. *Materials* **2021**, *14*, 4123. [CrossRef] [PubMed]
7. Googan, C. The cathodic protection potential criteria: Evaluation of the evidence. *Mater. Corros.* **2021**, *72*, 446–464. [CrossRef]
8. Msallamova, S.; Novak, P.; Kouril, M. Influence of cathodic protection on pH and change of soil electrolyte composition. In Proceedings of the METAL 2015 Conference, Brno, Czech Republic, 3–5 June 2015.

9. Wang, K.; Varela, F.B.; Tan, M.Y. The effect of electrode surface area on corrosion initiation monitoring of X65 steel in soil. *Corros. Sci.* **2019**, *152*, 218–225. [CrossRef]
10. Angst, U.; Büchler, M.; Martin, B.; Schöneich, H.-G.; Haynes, G.; Leeds, S.; Kajiyama, F. Cathodic protection of soil buried steel pipelines—A critical discussion of protection criteria and threshold values. *Mater. Corros.* **2016**, *67*, 1135–1142. [CrossRef]
11. Angst, U.M. A critical review of the science and engineering of cathodic protection of steel in soil and concrete. *Corrosion* **2019**, *75*, 1420–1433. [CrossRef]
12. Martinelli-Orlando, F.; Mundra, S.; Ansgt, U.M. Cathodic protection mechanism of iron and steel in porous media. *Commun. Mater.* **2024**, *5*, 15. [CrossRef]
13. Brenna, A.; Beretta, S.; Ormellese, M. AC corrosion of carbon steel under cathodic protection condition: Assessment, criteria and mechanism. A Review. *Materials* **2020**, *13*, 2158. [CrossRef] [PubMed]
14. Wang, H.; Du, C.; Liu, Z.; Ding, D. Effect of alternating current on the cathodic protection and interface structure of X80 steel. *Materials* **2017**, *10*, 851. [CrossRef] [PubMed]
15. Brenna, A.; Diamanti, M.V.; Lazzari, L.; Ormellese, M. A proposal of AC corrosion mechanism in cathodic protection. In Proceedings of the 2011 NSTI Nanotechnology Conference and Expo, Boston, MA, USA, 13–16 June 2011; pp. 553–556.
16. Brenna, A.; Ormellese, M.; Lazzari, L. Electro-mechanical breakdown mechanism of passive film in AC-related corrosion of carbon steel under cathodic protection condition. *Corrosion* **2016**, *72*, 1055–1063. [CrossRef] [PubMed]
17. Leeds, S.S.; Cottis, R.A. *An Investigation into the Influence of Surface Films on the Mechanism of Cathodic Protection*; CORROSION/2006, Paper No. 06084; National Association of Corrosion Engineers: Houston, TX, USA, 2006.
18. Leeds, S.S. A review of what happens at the metal/electrolyte interface when cathodic protection is applied. What does this all means in terms of the protection criterion? In Proceedings of the CEOCOR Conference, Firenze, Italy, 4–6 June 2013.
19. Barchiche, C.; Deslouis, D.; Gil, O.; Joiret, S.; Refait, P.; Tribollet, B. Role of sulphate ions on the formation of calcareous deposits on steel in artificial seawater: The formation of Green Rust compounds during cathodic protection. *Electrochim. Acta* **2009**, *54*, 3580–3588. [CrossRef]
20. Refait, P.; Jeannin, M.; Sabot, R.; Antony, H.; Pineau, S. Electrochemical formation and transformation of corrosion products on carbon steel under cathodic protection in seawater. *Corros. Sci.* **2013**, *71*, 32–36. [CrossRef]
21. Neale, C.N.; Hughes, J.B.; Ward, C.H. Impacts of unsaturated zone properties on oxygen transport and aquifer reaeration. *Ground Water* **2000**, *38*, 784–794. [CrossRef]
22. Cole, I.S.; Marney, D. The science of pipe corrosion: A review of the literature on the corrosion of ferrous metals in soils. *Corros. Sci.* **2012**, *56*, 5–16. [CrossRef]
23. Akkouche, R.; Rémazeilles, C.; Jeannin, M.; Barbalat, M.; Sabot, R.; Refait, P. Influence of soil moisture on the corrosion processes of carbon steel in artificial soil: Active area and differential aeration cells. *Electrochim. Acta* **2016**, *213*, 698–708. [CrossRef]
24. Akkouche, R.; Rémazeilles, C.; Barbalat, M.; Sabot, R.; Jeannin, M.; Refait, P. Electrochemical monitoring of steel/soil interfaces during wet/dry cycles. *J. Electrochem. Soc.* **2017**, *164*, 626–634. [CrossRef]
25. Azoor, R.M.; Deo, R.N.; Birbilis, N.; Kodikara, J. On the optimum soil moisture for underground corrosion in different soil types. *Corros. Sci.* **2019**, *159*, 108116. [CrossRef]
26. Akkouche, R.; Rémazeilles, C.; Jeannin, M.; Barbalat, M.; Refait, P. Corrosion of carbon steel in artificial soil: Processes occurring during wet/dry transitions studied with a multi-coupon electrode. *Electrochim. Acta* **2023**, *462*, 142745. [CrossRef]
27. Morcos, I. Double layer structure and the phenomena of wetting. *J. Colloid Interface Sci.* **1971**, *37*, 410. [CrossRef]
28. De Gennes, P.-G. Wetting: Statics and dynamics. *Rev. Mod. Phys.* **1985**, *57*, 827. [CrossRef]
29. Jin-Hua, C.; Shi-Hui, S.; Li-Hua, N.; Shou-Zhuo, Y. A novel method for rapid determination of PZC for solid metal/solution interface. *Electrochim. Acta* **1997**, *42*, 689.
30. Jiang, J.; Wang, J.; Lu, Y.-H.; Hu, J.-Z. Effect of length of gas/liquid/solid three-phase boundary (TPB) zone on cathodic and corrosion behavior of metals. *Electrochim. Acta.* **2009**, *54*, 1426. [CrossRef]
31. Stern, H.A.G.; Sadoway, D.R.; Tester, J.W. Copper sulfate reference electrode. *J. Electroanal. Chem.* **2011**, *659*, 143–150. [CrossRef]
32. *NF ISO 8407:2021*; Corrosion of Metals and Alloys—Removal of Corrosion Products from Corrosion Test Specimens. International Organization for Standardization (ISO): Geneva, Switzerland, 2021.
33. Zhang, X.L.; Jiang, Z.H.; Yao, Z.P.; Song, Y.; Wu, Z.D. Effects of scan rate on the potentiodynamic polarization curve obtained to determine the Tafel slopes and corrosion current density. *Corros. Sci.* **2009**, *51*, 581–587. [CrossRef]
34. Neff, D.; Dillmann, P.; Bellot-Gurlet, L.; Béranger, G. Corrosion of iron archaeological artefacts in soil: Characterization of the corrosion system. *Corros. Sci.* **2005**, *47*, 515–535. [CrossRef]
35. Deng, H.; Nanjo, H.; Qian, P.; Santosa, A.; Ishikawa, I.; Kurata, Y. Potential dependance of surface crystal structure of iron passive films in borate buffer solution. *Electrochim. Acta.* **2007**, *52*, 4272–4277. [CrossRef]
36. Refait, P.; Grolleau, A.-M.; Jeannin, M.; François, E.; Sabot, R. Localized corrosion of carbon steel in marine media: Galvanic coupling and heterogeneity of the corrosion product layer. *Corros. Sci.* **2016**, *111*, 583–595. [CrossRef]
37. Refait, P.; Géhin, A.; Abdelmoula, M.; Génin, J.-M.R. Coprecipitation thermodynamics of iron(II-III) hydroxysulphate green rust from Fe(II) and Fe(III) salts. *Corros. Sci.* **2003**, *45*, 656–676. [CrossRef]
38. Abd El Haleem, S.M.; Abd El Aal, E.E.; Abd El Wanees, S.; Diab, A. Environmental factors affecting the corrosion behaviour of reinforcing steel: I. The early stage of passive film formation in $Ca(OH)_2$ solutions. *Corros. Sci.* **2010**, *52*, 3875–3882. [CrossRef]

39. Abd El Haleem, S.M.; Abd El Wanees, S.; Abd El Aal, E.E.; Diab, A. Environmental factors affecting the corrosion behaviour of reinforcing steel: II. Role of some anions in the initiation and inhibition of pitting corrosion of steel in $Ca(OH)_2$ solutions. *Corros. Sci.* **2010**, *52*, 292–302. [CrossRef]
40. Harrington, S.P.; Wang, F.; Devine, T.M. The structure and electronic properties of passive and prepassive films of iron in borate buffer. *Electrochim. Acta.* **2010**, *55*, 4092–4102. [CrossRef]
41. Stern, M.; Geary, A.L. A theoretical analysis of the shape of polarization curves. *J. Electrochem. Soc.* **1957**, *104*, 56–63. [CrossRef]
42. Frankel, G.S. Electrochemical techniques in corrosion: Status, limitations, and needs. *J. ASTM Int.* **2008**, *5*, 101241. [CrossRef]